Ξ^- and Ω distributions in hadron–nucleus interactions

R. Vogt , T.D. Gutierrez

Abstract

Strange baryons have long been known to exhibit a leading particle effect. A recent comparison of Ξ^- production in π^-, n, and Σ^- interactions with nuclei show this effect clearly. These data are supplemented by earlier measurements of Ξ^- and Ω production by a Ξ^- beam. We calculate the Ξ^- and Ω x_F distributions and nuclear dependence in hA interactions using the intrinsic model.

PACS: 12.38.Lg; 13.85.Ni; 14.20.Jn

1. Introduction

Leading particle effects, flavor correlations between the final-state hadron and the projectile valence quarks, have long been observed in strange particle production. Although many experiments have recently focused on leading charm production [1–10], the first data involved strange particles [11–16]. With new data from the WA89 Collaboration on $\Xi^-(dss)$ production by $\pi^-(\bar{u}d)$, $n(udd)$, and $\Sigma^-(dds)$ projectiles on nuclear targets [17], in addition to Ξ^- production data from Ξ^- beams [14], doubly strange hadron production can be studied as a function of the number of strange valence quarks in the projectile. We compare our model calculations to both the x_F distributions and the integrated A

dependence reported by WA89 [17]. We also discuss Ξ^- and $\Omega(sss)$ production by the Ξ^- beam [14].

The WA89 Collaboration used carbon, C, and copper, Cu, targets to study the A dependence of Ξ^- production by π^-, n, and Σ^- beams [17]. The negative beams, π^- and Σ^-, had an average momentum of 345 GeV with a 9% momentum spread. The neutron beam had a lower momentum with a larger spread than the negative beams—the average momentum was 260 GeV with a 15% uncertainty. The detected Ξ^- was in the forward x_F region, $x_F \geqslant 0.05$, with low transverse momentum, $p_T \leqslant 2.5$ GeV. The data were parameterized in the form

$$\frac{d\sigma}{dp_T^2\, dx_F} \propto (1-x_F)^a e^{-bp_T^2}\ . \tag{1}$$

The pion and neutron results agree with the functional form of Eq. (1) over all x_F. For the pion, $a = 3.8 \pm 0.3$ for C and 4.1 ± 0.3 for Cu while for the neutron $a = 5.0 \pm 0.3$ for C and 4.8 ± 0.3 for Cu. These results are consistent with expectations from spectator counting rules [18], $d\sigma/dx_F \propto (1-x_F)^{2n_s-1}$. With an incident gluon, $n_s = 2$ for pions and 3 for neutrons, consistent with no leading particle effect for projectiles with zero strangeness. There is no significant A dependence of the exponent a.

On the other hand, the Σ^- data cannot be fit to Eq. (1) for $x_F < 0.4$. In the large x_F region, $a = 2.08 \pm 0.04$ for C and 1.97 ± 0.04 for Cu. These results indicate a very hard x_F distribution, inconsistent with the counting rules even for a valence quark since $n_s = 2$ gives $(1-x_F)^3$. In addition, at $x_F < 0.4$, the distribution is independent of x_F for both targets. Thus these data show a strong leading particle effect since the Ξ^- has two valence quarks in common with the Σ^-. The statistics are also sufficient for an observable A dependence in the fitted values of a.

The integrated A dependence was also reported by WA89 [17]. The A dependence of the total cross section is often parameterized as

$$\sigma_{pA} = \sigma_{pp} A^{\alpha}. \tag{2}$$

The integrated α for Σ^- production of Ξ^-, $\alpha = 0.679 \pm 0.011$ [17], is in relatively good agreement with previous fits. However, the pion and neutron data show a closer-to-linear A dependence, $\alpha = 0.891 \pm 0.034$ and 0.931 ± 0.046, respectively. WA89 attributes this difference to the fact that two $s\bar{s}$ pairs must be produced to make the final-state Ξ^- and $s\bar{s}$ pair production would be suppressed relative to light $q\bar{q}$ production.

WA89 has also measured the dependence of α on x_F. This dependence, $\alpha(x_F)$, was previously reported for a wide range of hadron projectiles [19]. For non-strange hadrons and hadrons with a single strange quark, there is a common trend with x_F. At $x_F = 0$, $\alpha \approx 0.8$ and decreases to ≈ 0.5 at large x_F, an overall decrease of $\sim A^{1/3}$ for $0 < x_F < 1$. The Ξ^0, the only doubly-strange hadron included in Ref. [19], is an exception. In pA interactions, the Ξ^0 has a larger value of α at low x_F [16]. A similar effect is observed for Ξ^- production by WA89. Their measurements of $\alpha(x_F)$ for Ξ^- from pion and neutron beams show that $\alpha \sim 1$ for $x_F \sim 0.05$, decreasing to $\alpha \sim 0.7$ at higher x_F. Thus the decrease of α with x_F is also $\approx A^{1/3}$ in this case although the actual values of α are larger than those for lighter hadrons [19]. However, for Σ^--induced Ξ^- production, $\alpha \sim 0.7$ almost independent of x_F.

The other data we consider are $\Xi^-\mathrm{Be} \to \Xi^-, \Omega$ at 116 GeV, measured by Biagi et al. [14]. In this case, the final-state Ξ^- x_F distribution increases with x_F, as does the Ω x_F distribution. This increase could be due in part to the use of an invariant parameterization [14],[1]

$$E\frac{d\sigma}{dp^3} \propto (1-x_F)^{a'} e^{-b' p_T^2}, \tag{3}$$

which fits the Ξ^- data at $x_F > 0.5$ but only approximately fits the Ω data in this limited region. The exponent a' was fit in two p_T^2 intervals, $p_T^2 < 0.4$ GeV^2 and $0.4 < p_T^2 < 2.9$ GeV^2, yielding $a' = -0.45 \pm 0.02$ and -0.18 ± 0.03, respectively. Between the most central measurement, $x_F = 0.15$, and the projectile fragmentation region, $x_F = 0.85$, the Ξ^- cross section increases by a factor of ~ 40 in the low p_T^2 interval.

A comparison of these results with incident proton data [14], $pA \to \Xi^- X$ [11,20] and $pA \to pX$ [21], showed that, at low x_F, Ξ^- production is essentially independent of the projectile while, at high x_F, the features of $\Xi^- A$ and pA scattering are similar. This behavior supports valence quark domination at high x_F. The structure of the Ω x_F distribution is similar: it is of the same order of magnitude as $pA \to \Omega X$ [11] at low x_F but is similar to singly strange baryon production by protons, $pA \to \Lambda X$, $\Sigma^+ X$ [11,20,22], at high x_F.

Since only one target was used, $\alpha = 0.6$ was assumed in Eq. (2) to obtain the per nucleon cross sections. This extrapolated cross section is a factor of 1.5–2 higher than those on hydrogen targets [14]. An extrapolation with $\alpha = 1$ gives better agreement with the hydrogen target data, at least for Ξ^- production.

We employ the intrinsic model [23–27], developed for strangeness production in Ref. [28]. In the intrinsic model, a hadron can fluctuate into Fock state configurations with a combination of light and strange quark pairs. The heavier quarks in the configuration are comoving with the other partons in the Fock state and thus can coalesce with these comoving partons to produce strange hadrons at large x_F. The model combines leading-twist production of $s\bar{s}$ pairs with intrinsic Fock states with up to nine particles. Thus coalescence production of the Ω from a proton is possible.

In Section 2, we describe leading-twist production of strange hadrons and explore some of the uncertainties in these calculations. Section 3 briefly describes the intrinsic model while section 4 discusses the A dependence of the combined model. In Section 5, we compare our calculated x_F and A dependencies with the Ξ^- and Ω data. Finally, in Section 6, we draw our conclusions.

2. Leading-twist production

We calculate leading-twist strangeness to leading order (LO) in perturbative QCD, assuming the strange quark is massive. We note, however, that quarks lighter than charm are difficult to treat perturbatively [29,30]. The strange quark is considerably lighter than

[1] For the two parameterizations to be equivalent, the right-hand side of Eq. (1) should be multiplied by $2E/\sqrt{s}$ to obtain the invariant cross section.

the charm quark, $m_s \approx 150$–500 MeV $\approx (1/10$–$1/3)m_c$. We cannot treat the lighter end of this mass range in our model at all since $m_s \sim 150$ MeV $\sim \Lambda_{\rm QCD}$. This mass is less than the minimum scale, μ_0, of all parton distribution functions and the strong coupling constant, α_s, blows up.

We choose proton parton distribution functions with the lowest possible initial scale μ_0 consistent with $m_s > \mu_0$. Therefore, the baryon parton distribution functions are based on the GRV 94 LO proton parton distributions [31] with $\mu_0^2 = 0.4$ GeV^2. We use the most recent pion parton densities by Glück et al. [32]. To be conservative, we assume that the scale μ at which the strong coupling constant and the parton densities are evaluated is $\mu = 2m_T$ where $m_T = \sqrt{p_T^2 + m_s^2}$ and $m_s = 500$ MeV. We will discuss the dependence of the leading twist results on these choices, albeit in a rather limited range. The x_F distributions, obtained by integrating Eq. (1) or (3) over p_T, are dominated by low p_T production.

We treat the strange quark as heavy, as in Ref. [28], rather than as a massless parton in jet-like processes. Treating the strange quark as a jet means selecting a minimum p_T to keep the cross section finite. A large minimum p_T compatible with hard scattering is incompatible with the assumption of intrinsic production, inherently a low p_T process [25]. Strange hadrons can either be produced directly in jet production or by the fragmentation of light quark and gluon jets. However, there is no indication that these data originate from jets. To test the dependence of our results on the production mechanism, we will also consider the possibility of flavor excitation, a jet-like process, when the projectile has non-zero strangeness.

We denote the leading-twist x_F distribution of heavy quark production [33] by F,

$$F \equiv \frac{d\sigma_{\rm ltf}^S}{dx_F} = \frac{\sqrt{s}}{2} \int dz_3\, dy_2\, dp_T^2\, x_a x_b H_{AB}\big(x_a, x_b, \mu^2\big) \begin{matrix} 1 & D_{S/s}(z_3) \\ E_1 & z_3 \end{matrix}, \tag{4}$$

where A and B are the initial hadrons, a and b are the interacting partons, 1 and 2 are the produced strange quarks and 3 is the final-state strange hadron S. The x_F of the detected strange quark is $x_F = 2m_T \sinh y_1/\sqrt{s}$ where y_1 is the rapidity of the strange quark and $\sqrt{s}$ is the hadron–hadron center of mass energy. We assume the simplest possible fragmentation function,

$$D_{S/s}(z) = B_S \delta(1-z), \tag{5}$$

with $B_S = 0.1$, assuming that all 10 ground-state strange hadrons are produced at the same rate to leading twist [28]. This choice of $D_{S/s}$ gives the hardest possible leading twist x_F distribution.

We define $H_{AB}(x_a, x_b, \mu^2)$ as the convolution of the subprocess $q\bar{q}$ annihilation and gluon fusion cross sections with the parton densities,

$$\begin{aligned} &H_{AB}\big(x_a, x_b, \mu^2\big) \\ &\quad = \sum_q \big[f_q^A\big(x_a, \mu^2\big) f_{\bar{q}}^B\big(x_b, \mu^2\big) + f_{\bar{q}}^A\big(x_a, \mu^2\big) f_q^B\big(x_b, \mu^2\big) \big] \frac{d\hat{\sigma}_{q\bar{q}}}{d\hat{t}} \\ &\qquad + f_g^A\big(x_a, \mu^2\big) f_g^B\big(x_b, \mu^2\big) \frac{d\hat{\sigma}_{gg}}{d\hat{t}}, \end{aligned} \tag{6}$$

where $q = u,\ d$, and s. Although including the s quark in the sum over q in Eq. (6) could lead to some over counting, the strange quark contribution to F from non-strange projectiles is negligible, less than 0.01% for neutron and pion projectiles. It is somewhat larger for strange projectiles, 2.5% for the Σ^- and 5.6% for the Ξ^-, but it is only significant at large x_F.

Hyperon parton distributions can be inferred from the proton distributions [27] by simple counting rules. We can relate the valence s distribution of the Σ^-, $f_{s_v}^{\Sigma^-}$, to the proton valence d distribution, $f_{d_v}^{p}$, and the valence d distribution in the Σ^-, $f_{d_v}^{\Sigma^-}$, to the valence u in the proton, $f_{u_v}^{p}$, so that

$$\int_0^1 dx\, f_{s_v}^{\Sigma^-}(x,\mu^2) = \int_0^1 dx\, f_{d_v}^{p}(x,\mu^2) = 1, \tag{7}$$

$$\int_0^1 dx\, f_{d_v}^{\Sigma^-}(x,\mu^2) = \int_0^1 dx\, f_{u_v}^{p}(x,\mu^2) = 2. \tag{8}$$

We also identify the up quark in the sea of the Σ^- with the strange quark in the proton sea, $f_u^{\Sigma^-}(x,\mu^2) = f_s^{p}(x,\mu^2)$. Similar relations hold for the antiquark distributions. Likewise, for the Ξ^-, we relate the valence s, $f_{s_v}^{\Xi^-}$, to the valence u in the proton, $f_{u_v}^{p}$, and equate the valence d distributions in both baryons so that,

$$\int_0^1 dx\, f_{s_v}^{\Xi^-}(x,\mu^2) = \int_0^1 dx\, f_{u_v}^{p}(x,\mu^2) = 2, \tag{9}$$

$$\int_0^1 dx\, f_{d_v}^{\Xi^-}(x,\mu^2) = \int_0^1 dx\, f_{d_v}^{p}(x,\mu^2) = 1. \tag{10}$$

Here also, $f_u^{\Xi^-}(x,\mu^2) = f_s^{p}(x,\mu^2)$. The gluon distributions are assumed to be identical for all baryons, $f_g^{p} = f_g^{\Sigma^-} = f_g^{\Xi^-}$. The leading order subprocess cross sections for heavy quark production can be found in Ref. [34]. The fractional momenta carried by the projectile and target partons, x_a and x_b, are $x_a = (m_T/\sqrt{s})(e^{y_1} + e^{y_2})$ and $x_b = (m_T/\sqrt{s})(e^{-y_1} + e^{-y_2})$.

The leading-twist x_F distributions with all four projectiles are shown in Fig. 1. (Note that B_S from Eq. (5) is included in the normalization.) We give the fusion x_F distributions, F, in $\pi^- p$ and $\Sigma^- p$ interactions at 345 GeV, np interactions at 260 GeV, and $\Xi^- p$ interactions at 116 GeV, corresponding to the energies we investigate. The $\pi^- p$ distribution is the broadest because the $f_{\bar{u}_v}^{\pi^-}(x_a) f_{u_v}^{p}(x_b)$ contribution hardens the x_F distribution at large x_F where the $q\bar{q}$ channel dominates.

To study the effect of parameter choice on F, we have varied m_s between 400 and 650 MeV, keeping $\mu = 2m_T$. The upper value is essentially too high for a realistic strange quark mass but it is included both for a larger range of m_s and to allow a comparison of scale choice between $\mu = m_T$ and $2m_T$. The ratios, $R(m_s,\mu)$ of F calculated with

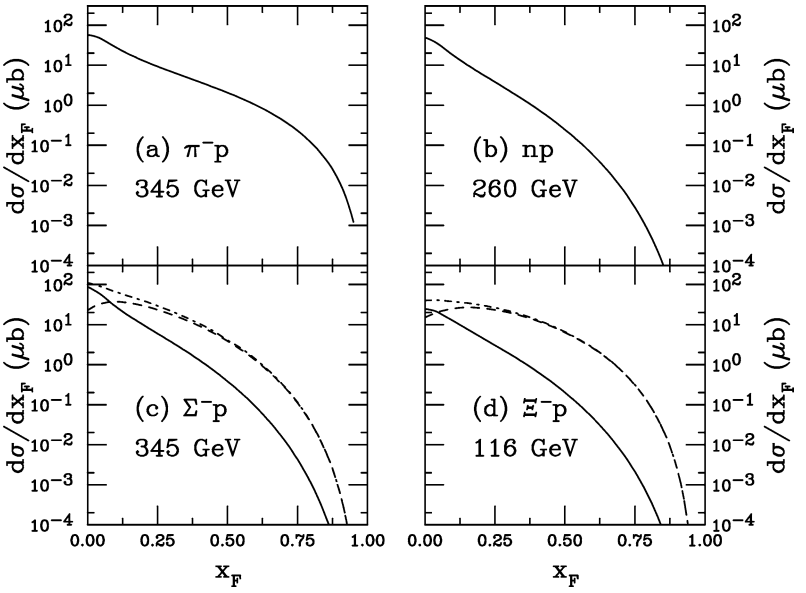

Fig. 1. Leading-twist strange quark production in (a) $\pi^- p$ interactions at 345 GeV, (b) np interactions at 260 GeV, (c) $\Sigma^- p$ interactions at 345 GeV, and (d) $\Xi^- p$ interactions at 116 GeV. The solid curves are the fusion results, F. For projectiles with valence strange quarks, the excitation contributions, $X_{p_{T_{\min}}}$ with $p_{T_{\min}} = 1$ GeV, are shown in the dashed curves. The dot-dashed curves are the total, $F + X_{p_{T_{\min}}}$.

$m_s = 400$ MeV and 650 MeV, relative to the default value of $m_s = 500$ MeV are shown in Fig. 2. Changing the mass strongly affects the total cross section but only weakly influences the shape of the x_F distributions. Reducing m_s increases the cross section by a factor of 2–3 while increasing m_s lowers the cross section by a similar factor.

We have also tried lowering the scale to m_T, more consistent with that used for heavier quarks. However, this is only possible for the top value of m_s considered above, 650 MeV. It is not clear how meaningful this comparison is because $\mu = m_T$ is quite close to μ_0, the minimum scale of the GRV 94 LO parton densities. Near μ_0, this set has a very rapid scale evolution which strongly affects the shape of the parton densities. We show $R(m_s, \mu)$ for $m_s = 650$ MeV and $\mu = m_T$ relative to $m_s = 650$ MeV and $\mu = 2m_T$ in the dot-dashed curves in Fig. 2. The scale dependence is large and strongly affects the ratios. The uncertainty in the evolution at low scales and the anomalously large strange quark mass makes these results useful only for illustrative purposes.

We have assumed only gg and $q\bar{q}$ contributions to massive strange quark production. We have also checked how the x_F distribution would change if the strange quark was treated as massless and all $2 \to 2$ scattering channels were included. Jet production of s quarks is through processes such as $gs \to gs$, $qs \to qs$ and $\bar{q}s \to \bar{q}s$. (Similarly for the $\bar{s}$.) Including these processes increases the cross section by a factor of 4–8. While this factor is not constant, it increases rather slowly with x_F so that the difference in shape is only important in the region where intrinsic production dominates, as discussed later.

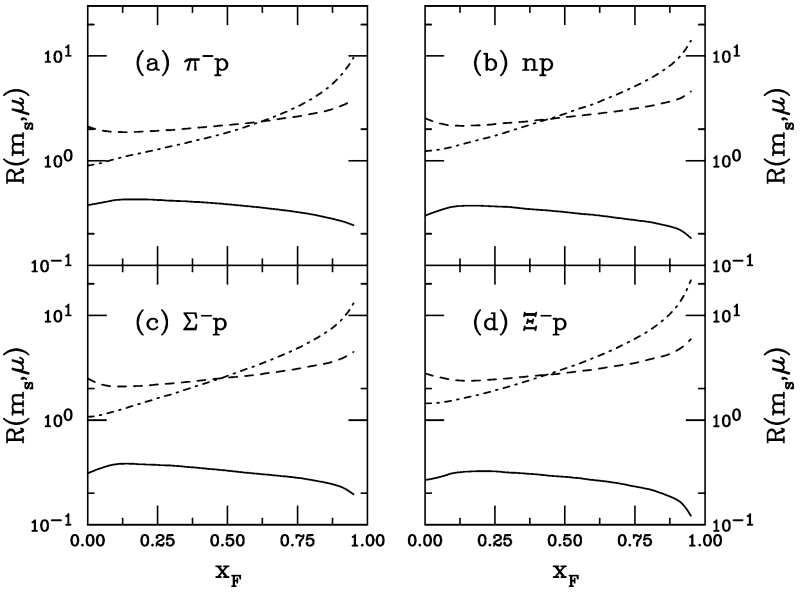

Fig. 2. We demonstrate how the parameter choice affects F by calculating the ratios $R(m_s, \mu)$. The solid and dashed curves are ratios to the defaults in Fig. 1, showing the mass dependence. The solid curves employ $m_s = 400$ MeV and $\mu = 2m_T$, the dashed curves, $m_s = 650$ MeV and $\mu = 2m_T$. The dot-dashed curves are calculations of the scale dependence. With $m_s = 650$ MeV, we form the ratio with $\mu = m_T$ to $\mu = 2m_T$. Results are shown for (a) $\pi^- p$ interactions at 345 GeV, (b) np interactions at 260 GeV, (c) $\Sigma^- p$ interactions at 345 GeV, and (d) $\Xi^- p$ interactions at 116 GeV.

Contributions from massless $2 \to 2$ scattering increase more rapidly at $x_F > 0$ for strange projectiles because the contribution from, for example, $f_s^{\Sigma^-}(x_a) f_g^p(x_b)$, dominates the scattering cross section. In the infinite momentum frame, $f_{s_v}^{\Sigma^-} = f_{d_v}^p$, see Eq. (8), and $f_{s_v}^{\Sigma^-}$ is large at large x_a while f_g^p increases as x_b decreases. To take this into account quantitatively, we have incorporated "flavor excitation" of massive strange valence quarks. The excitation matrix elements for massive quarks are found in Ref. [35]. The flavor excitation cross section has a pole when $p_T \to 0$ so that a cutoff, $p_{T_{\min}}$, is required to keep this cross section finite, as in jet production. We employ $p_{T_{\min}} = 2m_s = 1$ GeV. The leading-twist fusion cross section for strange projectiles is then augmented by

$$X_{p_{T_{\min}}} \equiv \frac{d\sigma_{\rm lte}^S}{dx_F} = \frac{\sqrt{s}}{2} \int dz_3\, dy_2\, dp_T^2\, x_a' x_b' H_{AB}'(x_a', x_b', \mu^2) \begin{matrix} 1 & D_{S/s}(z_3) \\ E_1 & z_3 \end{matrix}, \qquad (11)$$

where

$$H_{AB}'(x_a', x_b', \mu^2) = f_{s_v}^A(x_a', \mu^2) \left\{ \sum_q \left[f_q^B(x_b', \mu^2) + f_{\bar{q}}^B(x_b', \mu^2) \right] \frac{d\hat{\sigma}_{sq}}{d\hat{t}} + f_g^B(x_b', \mu^2) \frac{d\hat{\sigma}_{sg}}{d\hat{t}} \right\}, \qquad (12)$$

$x_a' = (m_T e^{y_1} + p_T e^{y_2})/\sqrt{s}$ and $x_b' = (m_T e^{-y_1} + p_T e^{-y_2})/\sqrt{s}$. Note that there is no overlap between the processes included in Eqs. (12) and (6) and thus no double counting. This

excitation mechanism is effective only for hadrons with a strange quark in the final state and thus does not affect the distributions with a produced $\bar{s}$.

To summarize, for strange and antistrange final states produced by non-strange hadrons,

$$\frac{d\sigma^S_{\rm lt}}{dx_F} = \frac{d\sigma^S_{\rm ltf}}{dx_F} \equiv F, \tag{13}$$

as in Eq. (4). This relation also holds for antistrange final states from strange hadrons. However, for strange hadron production by hadrons with non-zero strangeness, we also consider

$$\frac{d\sigma^S_{\rm lt}}{dx_F} = \frac{d\sigma^S_{\rm ltf}}{dx_F} + \frac{d\sigma^S_{\rm lte}}{dx_F} \equiv F + X_{p_{T_{\rm min}}}, \tag{14}$$

where flavor excitation, Eq. (11), may play a role.

We remark that the role of flavor excitation in heavy quark production, as outlined in Ref. [35], is questionable. It was first proposed as a LO contribution to the total cross section and, as such, could be rather large if the heavy quark distribution in the proton is significant. However, the heavy quark distribution in the proton is only non-zero above the threshold m_Q. In addition, parton distribution functions are defined in the infinite momentum frame where the partons are treated as massless. Later studies at next-to-leading order (NLO) [36] showed that these excitation diagrams are a subset of the NLO cross section and suppressed relative to fusion production. They are only a small fraction of the heavy flavor cross section and thus play no significant role at low energies. Strange hadron production at large x_F is then an important test of the excitation process.

Our calculations of $X_{p_{T_{\rm min}}}$ and $F + X_{p_{T_{\rm min}}}$ with $p_{T_{\rm min}} = 1$ GeV are shown in the dashed and dot-dashed curves, respectively, in Fig. 1. When excitation is considered, as in $\Sigma^- p$ and $\Xi^- p$ interactions, the x_F distribution is hardened, particularly through the $f_s^{\Sigma^-}(x'_a) f_g^p(x'_b)$ and $f_s^{\Xi^-}(x'_a) f_g^p(x'_b)$ contributions. These dominate at large x_F where $f_s^S(x'_a)$ is large for valence strange quarks and $f_g^p(x'_b)$ is large at small x'_b. The effect is even stronger for the Ξ^- since it has two valence strange quarks. Note that, except at small x_F, the total leading-twist cross section is equivalent to $X_{p_{T_{\rm min}}}$.

The hardening of the x_F distributions due to flavor excitation is illustrated in Fig. 3 for several values of $p_{T_{\rm min}}$. We display the ratio $R(p_{T_{\rm min}}) = X_{p_{T_{\rm min}}}/F$ for $p_{T_{\rm min}} = 1$ GeV (solid curves), 0.5 GeV (dashed curves) and 2 GeV (dot-dashed curves). Decreasing $p_{T_{\rm min}}$ by a factor of two increases $X_{p_{T_{\rm min}}}$ by an order of magnitude at low x_F. Note that $R(p_{T_{\rm min}})$ generally keeps increasing with x_F since F is softer and peaks at $x_F = 0$ while $X_{p_{T_{\rm min}}}$ peaks at $x_F \sim 0.25$, see Fig. 2. The growth of the ratio is not as strong when $p_{T_{\rm min}}$ is increased and, in fact, for $\Sigma^- p$ interactions at 345 GeV, $F > X_{p_{T_{\rm min}}}$ for all $x_F > 0$. The ratios are all larger for $\Xi^- p$ interactions at 116 GeV, due to both the increase of $X_{p_{T_{\rm min}}}$ with two strange valence quarks and the smaller F at the lower energy. Even the choice of $p_{T_{\rm min}} = 2$ GeV gives $X_{p_{T_{\rm min}}}/F > 1$ for $x_F > 0.25$.

We also remark that, since our calculation is LO, the light strange quark mass would mean quite large NLO corrections. The NLO K factor for charm production is a factor of two or more [37]. The NNLO corrections to the charm cross sections are also quite significant [30]. We can expect larger K factors for strange quark production. However, as we discuss later, the relative intrinsic to leading twist rate is the most important factor in

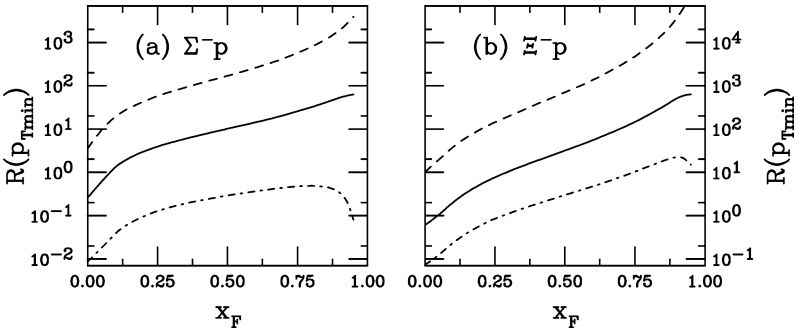

Fig. 3. We plot the ratio $R(p_{T_{\rm min}}) = X_{pT_{\rm min}}/F$ for $p_{T_{\rm min}} = 0.5$ GeV (dashed), 1 GeV (solid) and 2 GeV (dot-dashed). Results are shown for (a) $\Sigma^- p$ interactions at 345 GeV and (b) $\Xi^- p$ interactions at 116 GeV.

determining the success of the model. This relative factor can be adjusted to compensate for higher-order corrections as well as mass and scale variations.

Finally, we make an approximate estimate of the exponent a from Eq. (1) from the average x_F, $\langle x_F \rangle$, where

$$a = \frac{1}{\langle x_F \rangle} - 2, \tag{15}$$

as a simple comparison between the leading-twist calculations and the data. When the distributions shown in Fig. 1 are averaged over $x_F > 0$, the values of a obtained are larger than those measured by WA89, as expected. For the pion and neutron beams, $a = 5.2$ and 8.7, respectively. Strangeness production by strange hadrons including fusion alone also gives large values of a, 9 for the Σ^- and 7.4 for the Ξ^-. The x_F distribution of strange quarks produced by flavor excitation is considerably harder, $a = 3.2$ for the Σ^- and 2.2 for the Ξ^-. Combining the two contributions, as in the dot-dashed curves in Fig. 1(c) and (d), gives a somewhat larger value of a than for flavor excitation alone, $a = 4.7$ and 2.9 for Σ^- and Ξ^- beams, respectively. The values of a obtained from Eq. (15) are all much higher than those obtained from the data. Thus the leading twist results alone cannot explain the shape of the measured Ξ^- x_F distributions.

3. The intrinsic model for strangeness

We now briefly discuss the intrinsic model for strangeness production, described in detail for $\pi^- p$ interactions in Ref. [28]. Since all the data is at $x_F > 0$, we only discuss intrinsic production in the projectile.

The hadron wavefunction is a superposition of Fock state fluctuations in which the hadron contains one or more "intrinsic" $Q\overline{Q}$ pairs. These pairs can hadronize when the hadron interacts, breaking the coherence of the state. The model, first developed for charm [23,24], gives heavy quarks a larger fraction of the projectile momentum due to their greater mass. The strange quark is lighter so that the momentum gained is not as large. However, the intrinsic strangeness probability is larger, $P^5_{\rm is} \sim 2\%$. For simplicity, we

assume that the intrinsic probabilities are independent of the valence quark content of the projectile. Then $P^5_{\rm is}$ is identical for nucleons and hyperons. The Fock state probabilities for up to $3Q\overline{Q}$ pairs where at least one $Q\overline{Q}$ pair is strange are given in Ref. [28].

In this paper, we focus on $\Xi^-(dss)$ and $\Omega(sss)$ production from $\pi^-(\bar{u}d)$, $n(udd)$, $\Sigma^-(dds)$ and $\Xi^-(dss)$ projectiles. The produced Ξ^- shares one or more valence quarks with all the projectiles. We study Ω production only by Ξ^- projectiles, where two valence quarks are in common.

Once the coherence of the Fock state is broken, the partons in the state can hadronize in two ways. The first, uncorrelated fragmentation of the strange quark, is the same basic mechanism as at leading twist. However, when the Fock state fluctuation includes all the valence quarks of the final-state hadron, these quarks, in close spatial proximity and small relative velocity, can coalesce into the final-state hadron and come on shell. Thus, to calculate the full strange and antistrange hadron x_F distributions in the intrinsic model, we include uncorrelated fragmentation of the strange quark in every state considered and coalescence from those states where it is possible. In Ref. [28], comparison with strange baryon asymmetries suggested that fragmentation may not be an effective mechanism since it may cost too much energy when the Fock state has minimal invariant mass. This conclusion needs to be checked against inclusive x_F distributions over a broader x_F range.

In principle, the parton distributions of the hadron can be defined through such a Fock-state expansion [38]. In each fluctuation, only the mass distinguishes the light and heavy quark distributions. Thus it is not really possible in a given state to separate the "valence" and "sea" distributions. All are similar as long as the quarks are light. One distinguishing feature is our assumption that only strange quarks can produce strange final-state hadrons by uncorrelated fragmentation. Thus for hyperon projectiles, uncorrelated fragmentation may also be possible from Fock states with only light $Q\overline{Q}$ pairs. These intrinsic light quark states must be included in the total probability, as described in Ref. [28]. The probabilities for these states must also be defined. We assume

$$P^5_{\rm iq} = \left(\frac{\hat{m}_s}{\hat{m}_q}\right)^2 P^5_{\rm is} \approx 5\%, \tag{16}$$

$$P^7_{\rm iqq} = \left(\frac{\hat{m}_s}{\hat{m}_q}\right)^2 P^7_{\rm isq} = 1.75 P^5_{\rm is}, \tag{17}$$

$$P^9_{\rm iqqq} = \left(\frac{\hat{m}_s}{\hat{m}_q}\right)^4 P^9_{\rm issq} = 1.25 P^5_{\rm is}, \tag{18}$$

where we have used $\hat{m}_s = 0.71$ GeV and $\hat{m}_q = 0.45$ GeV for the effective transverse masses of the constituent partons in the Fock state. We further assume that the probabilities for the meson Fock configurations are equal to the baryon probabilities.

We remark that changing the parton masses in the intrinsic model does not strongly affect the shapes of the probability distributions of the final state hadrons. If $\hat{m} < 1$ GeV, changing the mass most strongly affects the independent fragmentation probability distributions since these depend only on the mass of the individual parton. However, when all the partons are combined in the hadron, as in coalescence, the effect is washed out since the x_F distribution depends primarily on the ratio of the number of quarks in the final-state hadron (2 for mesons, 3 for baryons) to the total number of quarks in the Fock

state. A comparison of the charm and strange quark and hadron probability distributions in Refs. [27,28], with $\hat{m}_c/\hat{m}_s \approx 2.6$, shows that the difference is small.

We have only taken the 10 ground state strange and antistrange hadrons into account. We assume that each hadron has a 10% probability for production by fragmentation, neglecting the particle masses. The final-state x_F distribution is then equivalent to that of the s or $\bar{s}$ quark. For coalescence, we count the number of strange and antistrange hadron combinations possible in a given Fock state and assign each strange hadron or antihadron that fraction of the total. The possible number of strange hadrons is greater than the number of possible antistrange hadrons. We clearly err in the overall normalization by simply including the ground state strange particles. However, the higher-lying resonances have the same quark content with the same fragmentation and coalescence distributions since all properties of the final-state hadrons except their quark content are neglected.

To obtain the total probability of each strange hadron produced from projectile hadron, h, in the intrinsic model, we sum the probabilities over all the states with up to 3 intrinsic $Q\overline{Q}$ pairs. Thus

$$\frac{dP_S^h}{dx_F} = \sum_n \sum_{r_u} \sum_{r_d} \sum_{r_s} \beta \begin{pmatrix} 1 & dP^{nF}_{\mathrm{i}(r_s\mathrm{s})(r_u\mathrm{u})(r_d\mathrm{d})} \\ 10 & dx_F \end{pmatrix} + \xi \frac{dP^{nC}_{\mathrm{i}(r_s\mathrm{s})(r_u\mathrm{u})(r_d\mathrm{d})}}{dx_F} \Bigg). \tag{19}$$

To conserve probability, $\beta = 1$ when the hadron is produced by uncorrelated fragmentation alone and 0.5 when both fragmentation and coalescence are possible. When we assume coalescence production only, we set $P^{nF} \equiv 0$ and $\beta \equiv 1$. The weight of each state produced by coalescence is ξ where $\xi = 0$ when S is not produced by coalescence from state $|n_v r_s(s\bar{s})r_u(u\bar{u})r_d(d\bar{d})\rangle$. The number of up, down and strange $Q\overline{Q}$ pairs is indicated by r_u, r_d and r_s, respectively. The total, $r_u + r_d + r_s = r$, is defined as $r = (n - n_v)/2$ because each Q in an n-parton state is accompanied by a $\overline{Q}$. For baryon projectiles, $n = 5$, 7, and 9 while for mesons $n = 4$, 6, and 8. Depending on the value of n, r_i can be 0, 1, 2 or 3, e.g., in a $|uuds\bar{s}d\bar{d}d\bar{d}\rangle$ state, $r_u = 0$, $r_d = 2$ and $r_s = 1$ with $r = 3$. Note that $r_s = 0$ is only possible when h is strange since no additional $s\bar{s}$ pairs are thus needed to produce some strange hadrons by coalescence. The total probability distributions, dP_S^h/dx_F, for $S = \Xi^-$ and Ω are given in Appendix A.

4. *A* dependence of combined model

The total x_F distribution for final-state strange hadron S is the sum of the leading-twist fusion and intrinsic strangeness components,

$$\frac{d\sigma^S_{hN}}{dx_F} = \frac{d\sigma^S_{\mathrm{lt}}}{dx_F} + \frac{d\sigma^S_{\mathrm{iQ}}}{dx_F}. \tag{20}$$

The leading-twist distributions are defined in Eqs. (13) and (14). The total intrinsic cross section, $d\sigma^S_{\mathrm{iQ}}/dx_F$, is related to dP_S^h/dx_F by

$$\frac{d\sigma^S_{\mathrm{iQ}}}{dx_F} = \sigma^{\mathrm{in}}_{hN} \frac{\mu^2_{\mathrm{iQ}}}{4\hat{m}_s^2} \frac{dP_S^h}{dx_F}. \tag{21}$$

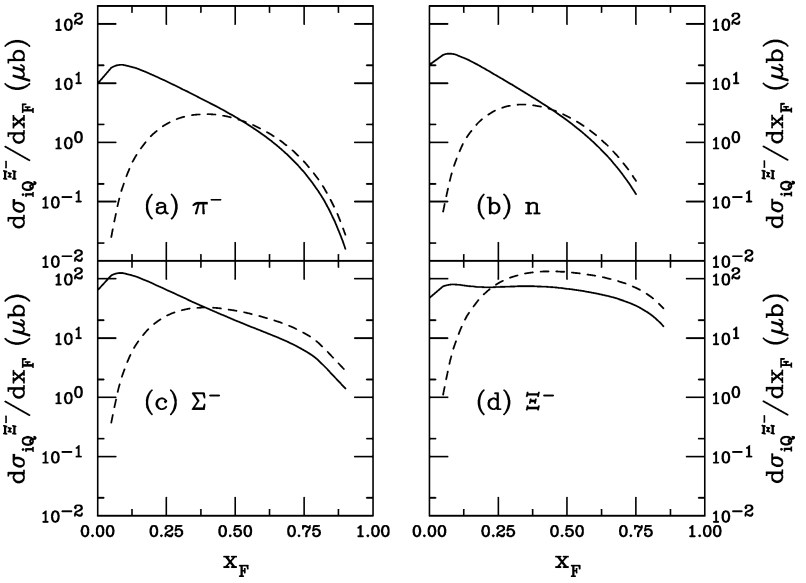

Fig. 4. The intrinsic model cross sections for Ξ^- production are shown for (a) π^-, (b) n, (c) Σ^- and (d) Ξ^- projectiles. The solid curves are the results with independent fragmentation and coalescence while the dashed curves are the results with coalescence alone.

The scale, $\mu_{\rm iQ}^2$, was fixed at 0.1 GeV^2 in intrinsic charm studies [27]. The inelastic hN cross sections are taken from the Particle Data Group parameterizations [39] and are evaluated at $\sqrt{s'} = \sqrt{s(1-|x_F|)}$ [26]. We have assumed that $\sigma^{\rm in}_{\Xi^- N} = \sigma^{\rm in}_{\Sigma^- N} \approx \sigma^{\rm in}_{\Lambda N}$. Thus $\sigma^{\rm in}_{\Xi^- N} = \sigma^{\rm in}_{\Sigma^- N} > \sigma^{\rm in}_{pN} > \sigma^{\rm in}_{\pi^- N}$.

We have fixed $\mu_{\rm iQ}^2$ to the value determined in Ref. [27]. However, it could be left as a free parameter to fit the data. Thus a change in m_s or μ in the leading-twist cross section could be compensated by a corresponding change in $\mu_{\rm iQ}^2$ to maintain a similar balance between the intrinsic and leading-twist cross sections.

In Fig. 4 we plot $d\sigma_{\rm iQ}^{\Xi^-}/dx_F$ for all projectiles considered. We show the results with independent fragmentation and coalescence (solid curves) and with coalescence alone (dashed curves). Independent fragmentation fills up the low x_F part of the probability but drops below the distributions with coalescence alone at high x_F due to the relative β in Eq. (19). The distributions with coalescence alone have a higher average x_F. A comparison of these distributions with the leading-twist results in Fig. 1 shows where each of the two contributions will dominate the total x_F distribution, Eq. (20).

We assume that the relative A dependence for leading-twist and intrinsic production is the same as that for heavy quarks and quarkonia [25,27,33,40]. The A dependence of the two component model is

$$\sigma_{hA} = A^{\gamma}\sigma_{\rm lt} + A^{\delta}\sigma_{\rm iQ}, \tag{22}$$

where the combination of the two terms should approximate A^{α} in Eq. (2). There are no strong nuclear effects on open charm at leading twist so that the A dependence is linear at

$x_F \sim 0$, $\alpha = 1$, [41], dropping to $\alpha = 0.77$ for pions and 0.71 for protons [33,42] at higher x_F where the intrinsic model begins to dominate. We assume that $\gamma = 1$ and $\delta = 0.77$ for pions and 0.71 for all baryons. Thus,

$$A^{\delta-\gamma} \approx A^{-1/3} \quad \text{as} \quad x_F \to 1. \tag{23}$$

This relative A dependence, similar to that discussed earlier for light hadrons [19], is included in our calculations. The proton and neutron numbers are taken into account in the calculation of the leading-twist cross section. This isospin effect is small for fusion, F, which is dominated by the gg channel. In perturbative QCD, $\gamma = 1$ could be modified by changes in the nuclear parton distributions relative to the proton [43]. However, the scale for our perturbative calculation is too low for such models of these modifications to apply [44,45] and are not included in our calculations.

5. Results

We begin by comparing the model to the WA89 pion data in Fig. 5. These data do not strongly distinguish between leading-twist fusion and the full model. The intrinsic results do not significantly depend on uncorrelated fragmentation. All three curves agree rather well with the data, primarily because the fusion x_F distribution is already fairly hard. Then the intrinsic contribution is a small effect even though the d valence quark is common between the π^- and the Ξ^-. The small intrinsic contribution is perhaps due to the fact that P^6_{iss} is already rather small, $\sim 0.6\%$. We note that the calculated total cross sections agree rather well with the measured ones despite the large uncertainties in the calculations.

Even though the intrinsic contribution is relatively small, as expected from a comparison of Fig. 1(a) with Fig. 4(a), it significantly affects the value of a obtained from Eq. (15). The difference between the a values found without and with uncorrelated fragmentation in the intrinsic model is negligible for the pion beam. We find $a \approx 4.1$ for the C target and 4.3 for the Cu target relative to $a = 5.2$ for leading twist alone. These results are within the errors

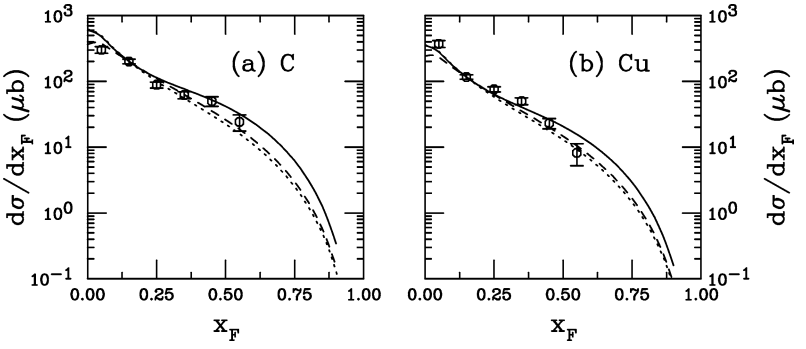

Fig. 5. The model is compared to the 345 GeV WA89 pion data on (a) C and (b) Cu targets. The dotted curves are leading-twist fusion, F, alone, the dashed curves include uncorrelated fragmentation and coalescence, and the solid curves include coalescence alone. The data sets have been normalized to the cross section per nucleon. The curves are normalized to the data at $x_F = 0.15$.

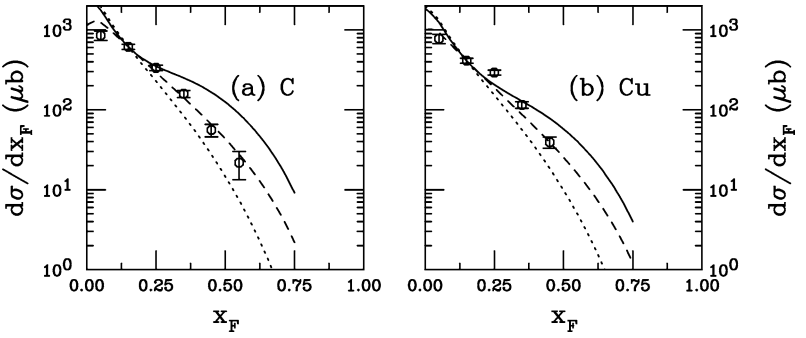

Fig. 6. The model is compared to the 260 GeV WA89 neutron data on (a) C and (b) Cu targets. The dotted curves are leading-twist fusion, F, alone, the dashed curves include uncorrelated fragmentation and coalescence, and the solid curves include coalescence alone. The data sets have been normalized to the cross section per nucleon. The curves are normalized to the data at $x_F = 0.15$.

of the WA89 fit to their data. The agreement is especially good since the two-component model does not give a smooth falloff as a function of x_F that can be easily quantified by a single exponent.

It is also possible to calculate $\alpha(x_F)$ and the x_F-integrated α from the ratios of the distributions for different values of A. The calculations including both uncorrelated fragmentation and coalescence generally give a smaller α and, hence, a stronger A dependence. This is because fragmentation peaks at low x_F, influencing the A dependence sooner than coalescence alone which is only significant at intermediate x_F. Thus $\alpha(x_F) \sim 0.9$ for fragmentation and coalescence while α decreases from ~ 1 at low x_F to 0.86 at high x_F with coalescence alone. The integrated values are 0.93 and 0.98, respectively, somewhat higher than the WA89 result but with the same general trend.

The overall agreement with the total cross section is not as good for the nA data, shown in Fig. 6. Surprisingly, the distribution including uncorrelated fragmentation agrees best with the data. This is perhaps because the energy of the secondary neutron beam is least well determined. The energy spread is 15% compared to 9% for the pion and Σ^- beams. A small energy variation can have a large effect on the leading-twist cross section. A 15% increase in the average neutron energy, from 260 GeV to 300 GeV, increases $d\sigma_{\rm lt}/dx_F$ by 80% at $x_F \sim 0.25$ while the intrinsic cross section is essentially unaffected. At 260 GeV the intrinsic cross section including both independent fragmentation and coalescence is equivalent to the fusion cross section at low x_F. On the other hand, the coalescence contribution is negligible at low x_F and begins to emerge at $x_F \approx 0.25$. A shift in the relative leading-twist and intrinsic production rates could easily reduce the effect of coalescence alone to be more compatible with the data. The uncertainty in the energy of the pion beam has a much weaker effect on the final result because the intrinsic contribution is already small, as is obvious from Fig. 5.

The calculated exponents a are larger for the neutron than the pion, in agreement with the WA89 measurements [17]. We find $a \approx 4.9$ for C and 5.8 for Cu. Typically the a obtained for fragmentation and coalescence is larger than that for coalescence alone since eliminating the fragmentation contribution tends to increase $\langle x_F \rangle$. The stronger A

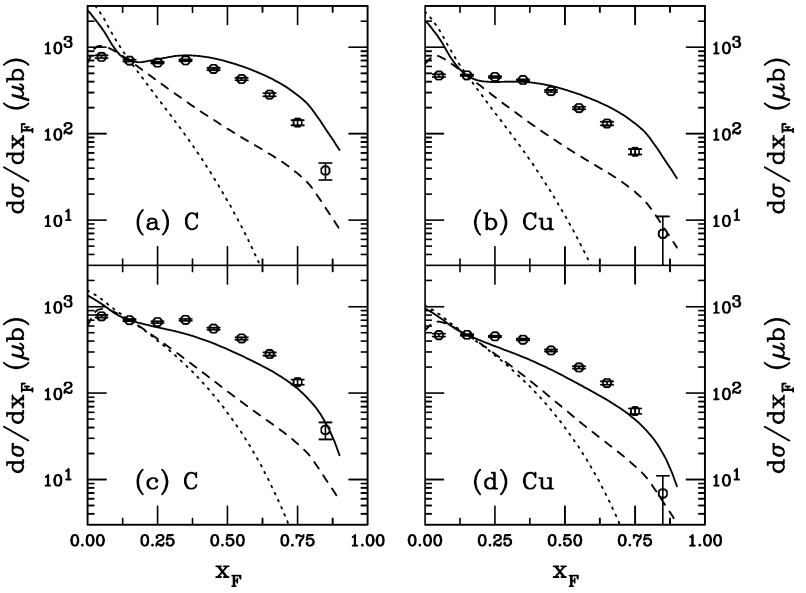

Fig. 7. The model is compared to the 345 GeV WA89 $\Sigma^- A$ data on C and Cu targets. In (a) and (b), the leading twist contribution is F while in (c) and (d), flavor excitation is also included, $F + X_{p_{T_{\min}}}$. The dotted curves are for leading-twist alone, the dashed curves include uncorrelated fragmentation and coalescence and the solid curves include coalescence alone. The data sets have been normalized to the cross section per nucleon. The curves are normalized to the data at $x_F = 0.15$.

dependence assumed for the intrinsic model has the effect of increasing a for larger nuclei. Thus the a found for the C target agrees rather well with the WA89 data while the Cu data suggest a harder distribution than our calculation implies. There is, however, a stronger A dependence in our calculation than in the data since the measured values of a for the two targets are less than one standard deviation apart. This stronger A dependence is reflected in the calculated values of α, 0.87 when fragmentation and coalescence are included and 0.95 with coalescence alone.

Even though there is some A dependence in the model calculations, the relatively small intrinsic contribution to the pion and neutron data leads to a rather weak overall A dependence. Dominance of the leading-twist cross section at low to intermediate x_F results in a nearer-to-linear integrated α, as observed by WA89 [17].

We now turn to Ξ^- production by the Σ^- where the A dependence can be expected to be stronger. For the first time, we have a valence strange quark in the projectile so that we can compare the effectiveness of fusion alone with flavor excitation. We can also better test the importance of uncorrelated fragmentation because coalescence production is already possible in the 5-parton Fock state, $|ddss\bar{s}\rangle$.

Our results are collected in Fig. 7. We first discuss the importance of uncorrelated fragmentation to leading-twist fusion, F, alone, Fig. 7(a) and (b). The leading-twist contribution is rather steeply falling. Including both uncorrelated fragmentation and coalescence broadens the x_F distribution but cannot match the hardness of the measured

x_F distribution. Eliminating the fragmentation contribution produces a much harder distribution for $x_F \geqslant 0.15$, matching the shape of the data relatively well.

The calculations are all normalized to the $x_F = 0.15$ point to more easily compare the shapes of the distributions. Including fragmentation gives better agreement at low x_F because uncorrelated fragmentation peaks close to $x_F \sim 0$, filling in the low to intermediate x_F range. Coalescence, on the other hand, always produces strange hadrons with $\langle x_F \rangle \geqslant 0.3$, broadening the distribution only in this region. Thus without fragmentation the calculations overestimate the data at $x_F \sim 0$. The data seem to indicate that uncorrelated fragmentation is not an effective mechanism for intrinsic production, in agreement with the conclusions of Ref. [28].

The agreement of the data with the solid curves in Fig. 7(a) and (b) is good but not perfect. The calculation overestimates the data at high x_F. Recall that for the neutron, the 15% spread in the beam momentum could result in an overestimate of the intrinsic contribution, as previously discussed. Although the possible spread in the Σ^- beam momentum is smaller, it could affect the relative intrinsic contribution at low to intermediate x_F. At large x_F, the effect on the shape would be negligible because the intrinsic contribution dominates. Thus, given the inherent uncertainties in the model and the data, the agreement is rather satisfactory.

We have obtained the values of a from $\langle x_F \rangle$, both over all x_F and for $x_F > 0.1$, avoiding the strong change in slope of the solid curves when coalescence alone is included in the intrinsic result. When we integrate over $x_F > 0$, $a = 3.02$ for C and 3.39 for Cu with both uncorrelated fragmentation and coalescence while with coalescence alone, $a = 1.24$ for C and 1.78 for Cu. Considering only the range $x_F > 0.1$, we find $a = 1.56$ for C and 1.63 for Cu with fragmentation and 0.43 for C, 0.57 for Cu without fragmentation. The calculated as suggest considerably harder x_F distributions in the more limited x_F region, particularly when coalescence alone is considered. However, none of the results are in good agreement with $a \approx 2$, as obtained by WA89 for $x_F \geqslant 0.4$. This is not surprising since the solid curve is harder than the data for $x_F > 0.1$. In any case, the coalescence contributions are difficult to fit to a power law since they approach zero at both $x_F = 0$ and $x_F = 1$ with a peak at intermediate x_F, see Fig. 4. The various contributions, all with somewhat different magnitudes due to the relative probabilities, peak at different values of x_F, complicating the situation further.

Calculations of α give $\alpha \approx 0.8$ for the integrated cross sections but $\alpha \approx 0.7$ for $x_F > 0.4$, with and without fragmentation in the intrinsic model, rather consistent with the WA89 result. However, as a function of x_F, coalescence alone is more consistent with the measurements since $\alpha \approx 1$ at $x_F \approx 0$, decreasing to 0.71 as $x_F \to 1$, as expected from Eq. (22).

We now check if our results improve when we include flavor excitation, Eq. (14), shown in Fig. 7(c) and (d). Now the baseline leading twist distribution, $F + X_{p_{T_{\min}}}$, is harder than F alone, as shown in Fig. 1(c). However, although the distribution is broader, it still drops six orders of magnitude over the entire x_F range with $p_{T_{\min}} = 1$ GeV while the intrinsic contribution with coalescence alone changes only by a factor of 10 for $x_F > 0.3$, see Fig. 4(c). Indeed, at these values of x_F, the intrinsic contribution is larger than both F and $F + X_{p_{T_{\min}}}$. Thus including flavor excitation also cannot describe the data without the intrinsic coalescence component, as in Fig. 7(a) and (b).

The total cross section is in reasonable agreement with that measured by WA89. Decreasing $p_{T_{\min}}$ further can harden the distribution but still cannot describe the shape of the data. A lower $p_{T_{\min}}$ enhances the total cross sections considerably so that, if $p_{T_{\min}} = 0.25$ GeV, the cross section is overestimated by several orders of magnitude. The intrinsic contribution is then negligible and decreasing $p_{T_{\min}}$ actually degrades the agreement with the data. Increasing $p_{T_{\min}}$ also cannot improve the agreement since the excitation contribution does not significantly harden the leading-twist x_F distribution. Thus there is no clear evidence for flavor excitation.

The trends in the A dependence are similar when excitation is included although the values of a obtained are suggestive of harder x_F distributions than with leading-twist fusion alone. In particular, the excitation contribution is harder at low x_F, see Fig. 1, causing the change in slope due to the hardening of the intrinsic distribution with coalescence alone to be less abrupt. Nonetheless, the agreement with the measured value of a is not significantly improved. The calculated values of $\alpha(x_F)$ are similar to those with leading-twist fusion alone but the integrated values of α are somewhat larger, ≈ 0.87, due to the larger leading-twist baseline. Thus the A dependence also does not suggest that flavor excitation is a significant contribution to strange hadron production.

To summarize, the A dependence of Ξ^- production by Σ^- is stronger because the intrinsic contribution with coalescence dominates the x_F distribution already at $x_F \sim 0.1$. Therefore the integrated A dependence is reduced nearly a factor of $A^{1/3}$ relative to the pion and neutron data, as shown in Eqs. (22) and (23). Thus the trends of the model are in agreement with the WA89 data.

Finally, we compare our intrinsic model calculations with the invariant Ξ^- and Ω cross sections measured in Ξ^-Be interactions at 116 GeV [14]. Since intrinsic production is expected to be a low p_T effect [25], we only compare to the low p_T^2 bin, $0 < p_T^2 < 0.4$ GeV^2 [46]. The data and our calculations are shown in Fig. 8. We have multiplied our x_F distributions by $2m_T \cosh y_1/\sqrt{s}$ to obtain the invariant cross section. The invariant x_F distributions are harder as a function of x_F.

Because the initial and final states are identical for Ξ^- production, the intrinsic contribution increases with x_F. However, even with coalescence alone, the increase does not continue beyond $x_F \sim 0.4$. A similar but weaker effect is seen for the Ω where there are two strange quarks in common with the Ξ^-. Therefore, we have tried to identify a mechanism that would increase the cross section beyond $x_F \sim 0.4$. One possibility is a "Pomeron-like" parton in the Fock state. Since the Pomeron has quantum numbers similar to two gluons, it can be exchanged between two projectile valence quarks. A $|dss\mathcal{P}\rangle$ state, where $\mathcal{P}$ signifies the "Pomeron", would result in Ξ^- states at high x_F while avoiding the $\delta(1-x_F)$ delta function for the 3-particle Fock state. A Ξ^- from such a configuration would have a distribution peaking at $x_F \to 1$. It is also possible to imagine a $|dsss\bar{s}\mathcal{P}\rangle$ state from which both the Ξ^- and Ω could be produced. In this case, the distribution would peak away from $x_F \sim 1$. We included "Pomeron" production from both states assuming that $P^4_{\mathrm{i}\mathcal{P}} = P^5_{\mathrm{iq}} \sim 5\%$ and that $P^6_{\mathrm{is}\mathcal{P}} = P^7_{\mathrm{iqq}} \sim 3.5\%$, giving these configurations large probability. The results, shown in the dot-dashed curves in Fig. 8, agree relatively well with the data, especially for the Ξ^-. The Ω data are still underestimated but the trend is now in the right direction.

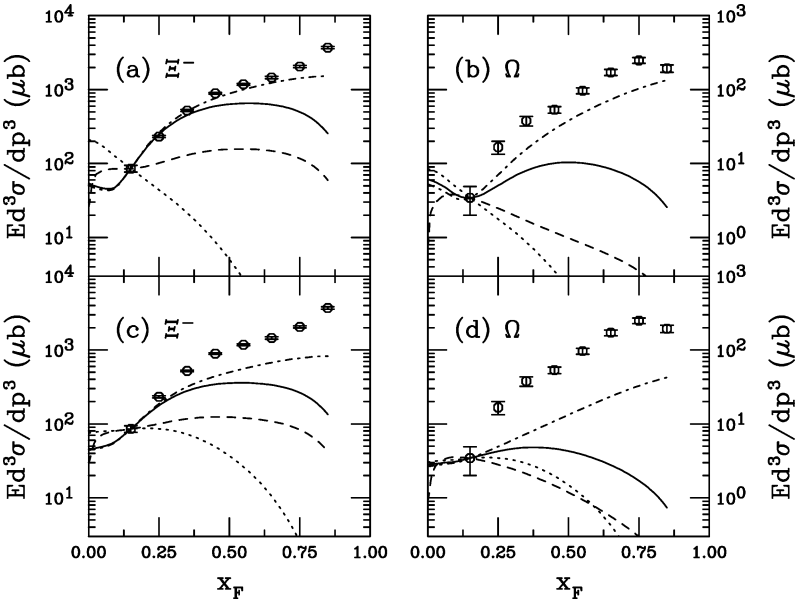

Fig. 8. The model is compared to the 116 GeV Ξ^-Be data. In (a) and (b), the leading twist contribution is F while in (c) and (d), flavor excitation is also included, $F + X_{p_{T_{\rm min}}}$. The dotted curves are for leading-twist fusion alone, the dashed curves include uncorrelated fragmentation and coalescence, the solid curves include coalescence alone and the dot-dashed curves include a diffractive "Pomeron" contribution. The data sets have been normalized to the cross section per nucleon. The curves are normalized to the data at $x_F = 0.15$.

Of course, this "Pomeron" is a rather artificial solution, especially when the initial and final states are not identical. If it is correct, it should also be included in $\Sigma^- p \to \Xi^- X$ calculations shown in Fig. 7. We have checked this process and found that the resulting x_F distribution is far too hard. Therefore, the practicality of the mechanism is questionable and the "Pomeron" results should not be taken too seriously.

Our calculations with flavor excitation are compared to the data in Fig. 8(c) and (d). The results do not improve, even when the "Pomeron" is included. Indeed, the results with excitation underestimate the shape of the data at high x_F more than with fusion alone. Decreasing $p_{T_{\rm min}}$ increases the leading-twist contribution, reducing the agreement with the shape of the distribution. Increasing $p_{T_{\rm min}}$ gives results very similar to those in Fig. 8(a) and (b) since the intrinsic contribution is again dominant. Therefore we conclude that flavor excitation is not an effective mechanism for strange hadron production at low p_T. This conclusion is consistent with the interpretation of the excitation diagrams as NLO contributions to the production cross section, as discussed previously.

We have also calculated the exponent a', see Eq. (3), for these distributions with $x_F > 0.5$. The results are negative for all the cases shown. We find $a' \approx -0.45$ with and without uncorrelated fragmentation and -0.5 with the "Pomeron". These values are rather consistent with those obtained for the low p_T^2 selection of the Ξ^- data. The corresponding values for Ω production are somewhat lower, ≈ -0.41, without the "Pomeron" but somewhat higher, ≈ -0.54, with it.

6. Conclusions

We have compared our intrinsic calculations to Ξ^- production by π^-, n and Σ^- projectiles and to Ξ^- and Ω production by Ξ^- projectiles. We find good agreement with the WA89 data for leading-twist fusion and coalescence using our default parameters. Large uncertainties exist in the leading-twist cross sections, as shown in Section 2. However, the most important parameter is $\mu^2_{\rm iQ}$ in the intrinsic cross section, Eq. (21), which fixes the relative leading-twist and intrinsic contributions. Then large changes in the leading-twist cross section due to uncertainties in mass or scale can be reduced by rescaling $\mu^2_{\rm iQ}$. We showed that changing the parameters in the leading-twist cross section does not significantly affect the shape of the x_F distributions, only their overall magnitude, except when the scale approaches μ_0. Thus, with appropriate rescaling of the relative contributions through $\mu^2_{\rm iQ}$, the intrinsic contribution will still dominate the x_F distributions at intermediate and large x_F, leaving the agreement with the data unchanged except for an overall normalization factor.

We have also excluded flavor excitation as a significant mechanism of low p_T strange hadron production. This conclusion is in agreement with results for heavier flavors like charm and bottom. The apparent difficulties with uncorrelated fragmentation seen in Ref. [28] are confirmed here. Thus coalescence production is the most effective mechanism for strange hadron production in the intrinsic model. The leading charm analysis should perhaps be revisited in light of this conclusion.

The conclusions that can be reached from the Ξ^--induced interactions at 116 GeV are less clear. It is possible that a "Pomeron"-like state could exist in the hadron wavefunction but its applicability to Ω production is somewhat doubtful. Therefore the interpretation of these data within the intrinsic model is rather inconclusive. More standard studies of diffractive production in $\Xi^-\mathrm{Be} \to \Xi^- X$ should be performed.

Acknowledgements

We thank P. Hoyer for reminding us of these data. R.V. would like to thank the Niels Bohr Institute and the Grand Accelerateur National d'Ions Lourds for hospitality at the beginning of this work.

Appendix A

Here we give the relevant probability distributions in the intrinsic model for Ξ^- and Ω production used in our calculations. To more clearly distinguish between the probability distributions including uncorrelated fragmentation and coalescence and those with coalescence alone, both distributions are given. The probability distribution with both contributions is given first, followed by that with coalescence alone.

First, we give the distributions relevant to the WA89 measurements. We reproduce the Ξ^- probability distribution from a π^- [28],

$$\frac{dP^{\pi^-}_{\Xi^-}}{dx_F} = \frac{1}{10}\frac{dP^{4F}_{\rm is}}{dx_F} + \frac{1}{10}\frac{dP^{6F}_{\rm isu}}{dx_F} + \frac{1}{10}\frac{dP^{6F}_{\rm isd}}{dx_F} + \frac{1}{2}\left(\frac{1}{10}\frac{dP^{6F}_{\rm iss}}{dx_F} + \frac{1}{7}\frac{dP^{6C}_{\rm iss}}{dx_F}\right) + \frac{1}{10}\frac{dP^{8F}_{\rm isuu}}{dx_F} + \frac{1}{10}\frac{dP^{8F}_{\rm isud}}{dx_F} + \frac{1}{10}\frac{dP^{8F}_{\rm isdd}}{dx_F} + \frac{1}{2}\left(\frac{1}{10}\frac{dP^{8F}_{\rm issu}}{dx_F} + \frac{1}{12}\frac{dP^{8C}_{\rm issu}}{dx_F}\right) + \frac{1}{2}\left(\frac{1}{10}\frac{dP^{8F}_{\rm issd}}{dx_F} + \frac{2}{12}\frac{dP^{8C}_{\rm issd}}{dx_F}\right) + \frac{1}{2}\left(\frac{1}{10}\frac{dP^{8F}_{\rm isss}}{dx_F} + \frac{3}{16}\frac{dP^{8C}_{\rm isss}}{dx_F}\right), \tag{A.1}$$

$$\frac{dP^{\pi^-}_{\Xi^-}}{dx_F} = \frac{1}{7}\frac{dP^{6C}_{\rm iss}}{dx_F} + \frac{1}{12}\frac{dP^{8C}_{\rm issu}}{dx_F} + \frac{2}{12}\frac{dP^{8C}_{\rm issd}}{dx_F} + \frac{3}{16}\frac{dP^{8C}_{\rm isss}}{dx_F}. \tag{A.2}$$

From a neutron projectile,

$$\frac{dP^{n}_{\Xi^-}}{dx_F} = \frac{1}{10}\frac{dP^{5F}_{\rm is}}{dx_F} + \frac{1}{10}\frac{dP^{7F}_{\rm isu}}{dx_F} + \frac{1}{10}\frac{dP^{7F}_{\rm isd}}{dx_F} + \frac{1}{2}\left(\frac{1}{10}\frac{dP^{7F}_{\rm iss}}{dx_F} + \frac{1}{13}\frac{dP^{7C}_{\rm iss}}{dx_F}\right) + \frac{1}{10}\frac{dP^{9F}_{\rm isuu}}{dx_F} + \frac{1}{10}\frac{dP^{9F}_{\rm isud}}{dx_F} + \frac{1}{10}\frac{dP^{9F}_{\rm isdd}}{dx_F} + \frac{1}{2}\left(\frac{1}{10}\frac{dP^{9F}_{\rm issu}}{dx_F} + \frac{2}{22}\frac{dP^{9C}_{\rm issu}}{dx_F}\right) + \frac{1}{2}\left(\frac{1}{10}\frac{dP^{9F}_{\rm issd}}{dx_F} + \frac{3}{22}\frac{dP^{9C}_{\rm issd}}{dx_F}\right) + \frac{1}{2}\left(\frac{1}{10}\frac{dP^{9F}_{\rm isss}}{dx_F} + \frac{6}{28}\frac{dP^{9C}_{\rm isss}}{dx_F}\right), \tag{A.3}$$

$$\frac{dP^{n}_{\Xi^-}}{dx_F} = \frac{1}{13}\frac{dP^{7C}_{\rm iss}}{dx_F} + \frac{2}{22}\frac{dP^{9C}_{\rm issu}}{dx_F} + \frac{3}{22}\frac{dP^{9C}_{\rm issd}}{dx_F} + \frac{6}{28}\frac{dP^{9C}_{\rm isss}}{dx_F}. \tag{A.4}$$

The Ξ^- distribution from a Σ^- projectile is,

$$\frac{dP^{\Sigma^-}_{\Xi^-}}{dx_F} = \frac{1}{10}\frac{dP^{5F}_{\rm iu}}{dx_F} + \frac{1}{10}\frac{dP^{5F}_{\rm id}}{dx_F} + \frac{1}{2}\left(\frac{1}{10}\frac{dP^{5F}_{\rm is}}{dx_F} + \frac{2}{6}\frac{dP^{5C}_{\rm is}}{dx_F}\right) + \frac{1}{10}\frac{dP^{7F}_{\rm iuu}}{dx_F} + \frac{1}{10}\frac{dP^{7F}_{\rm iud}}{dx_F} + \frac{1}{10}\frac{dP^{7F}_{\rm idd}}{dx_F} + \frac{1}{2}\left(\frac{1}{10}\frac{dP^{7F}_{\rm isu}}{dx_F} + \frac{1}{13}\frac{dP^{7C}_{\rm isu}}{dx_F}\right) + \frac{1}{2}\left(\frac{1}{10}\frac{dP^{7F}_{\rm isd}}{dx_F} + \frac{3}{13}\frac{dP^{7C}_{\rm isd}}{dx_F}\right) + \frac{1}{2}\left(\frac{1}{10}\frac{dP^{7F}_{\rm iss}}{dx_F} + \frac{6}{16}\frac{dP^{7C}_{\rm iss}}{dx_F}\right) + \frac{1}{10}\frac{dP^{9F}_{\rm iuuu}}{dx_F} + \frac{1}{10}\frac{dP^{9F}_{\rm iuud}}{dx_F} + \frac{1}{10}\frac{dP^{9F}_{\rm iudd}}{dx_F} + \frac{1}{10}\frac{dP^{9F}_{\rm iddd}}{dx_F} + \frac{1}{2}\left(\frac{1}{10}\frac{dP^{9F}_{\rm isuu}}{dx_F} + \frac{2}{22}\frac{dP^{9C}_{\rm isuu}}{dx_F}\right) + \frac{1}{2}\left(\frac{1}{10}\frac{dP^{9F}_{\rm isud}}{dx_F} + \frac{3}{22}\frac{dP^{9C}_{\rm isud}}{dx_F}\right) + \frac{1}{2}\left(\frac{1}{10}\frac{dP^{9F}_{\rm isdd}}{dx_F} + \frac{14}{22}\frac{dP^{9C}_{\rm isdd}}{dx_F}\right) + \frac{1}{2}\left(\frac{1}{10}\frac{dP^{9F}_{\rm issu}}{dx_F} + \frac{6}{28}\frac{dP^{9C}_{\rm issu}}{dx_F}\right) + \frac{1}{2}\left(\frac{1}{10}\frac{dP^{9F}_{\rm issd}}{dx_F} + \frac{9}{28}\frac{dP^{9C}_{\rm issd}}{dx_F}\right) + \frac{1}{2}\left(\frac{1}{10}\frac{dP^{9F}_{\rm isss}}{dx_F} + \frac{12}{32}\frac{dP^{9C}_{\rm isss}}{dx_F}\right), \tag{A.5}$$

$$\frac{dP^{\Sigma^-}_{\Xi^-}}{dx_F} = \frac{2}{6}\frac{dP^{5C}_{\rm is}}{dx_F} + \frac{1}{13}\frac{dP^{7C}_{\rm isu}}{dx_F} + \frac{3}{13}\frac{dP^{7C}_{\rm isd}}{dx_F} + \frac{6}{16}\frac{dP^{7C}_{\rm iss}}{dx_F} + \frac{2}{22}\frac{dP^{9C}_{\rm isuu}}{dx_F} + \frac{3}{22}\frac{dP^{9C}_{\rm isud}}{dx_F} + \frac{14}{22}\frac{dP^{9C}_{\rm isdd}}{dx_F} + \frac{6}{28}\frac{dP^{9C}_{\rm issu}}{dx_F} + \frac{9}{28}\frac{dP^{9C}_{\rm issd}}{dx_F} + \frac{12}{32}\frac{dP^{9C}_{\rm isss}}{dx_F}. \tag{A.6}$$

We now present the relevant probability distributions for Ξ^- and Ω production from a Ξ^- projectile. First we give the Ξ^- distributions,

$$\begin{aligned}
\frac{dP^{\Xi^-}_{\Xi^-}}{dx_F} &= \frac{1}{2}\left(\frac{1}{10}\frac{dP^{5F}_{\rm iu}}{dx_F} + \frac{1}{6}\frac{dP^{5C}_{\rm iu}}{dx_F}\right) + \frac{1}{2}\left(\frac{1}{10}\frac{dP^{5F}_{\rm id}}{dx_F} + \frac{2}{6}\frac{dP^{5C}_{\rm id}}{dx_F}\right) \\
&+ \frac{1}{2}\left(\frac{1}{10}\frac{dP^{5F}_{\rm is}}{dx_F} + \frac{3}{7}\frac{dP^{5C}_{\rm is}}{dx_F}\right) + \frac{1}{2}\left(\frac{1}{10}\frac{dP^{7F}_{\rm iuu}}{dx_F} + \frac{1}{13}\frac{dP^{7C}_{\rm iuu}}{dx_F}\right) \\
&+ \frac{1}{2}\left(\frac{1}{10}\frac{dP^{7F}_{\rm iud}}{dx_F} + \frac{2}{13}\frac{dP^{7C}_{\rm iud}}{dx_F}\right) + \frac{1}{2}\left(\frac{1}{10}\frac{dP^{7F}_{\rm idd}}{dx_F} + \frac{3}{13}\frac{dP^{7C}_{\rm idd}}{dx_F}\right) \\
&+ \frac{1}{2}\left(\frac{1}{10}\frac{dP^{7F}_{\rm isu}}{dx_F} + \frac{3}{16}\frac{dP^{7C}_{\rm isu}}{dx_F}\right) + \frac{1}{2}\left(\frac{1}{10}\frac{dP^{7F}_{\rm isd}}{dx_F} + \frac{6}{16}\frac{dP^{7C}_{\rm isd}}{dx_F}\right) \\
&+ \frac{1}{2}\left(\frac{1}{10}\frac{dP^{7F}_{\rm iss}}{dx_F} + \frac{6}{17}\frac{dP^{7C}_{\rm iss}}{dx_F}\right) + \frac{1}{2}\left(\frac{1}{10}\frac{dP^{9F}_{\rm iuuu}}{dx_F} + \frac{1}{22}\frac{dP^{9C}_{\rm iuuu}}{dx_F}\right) \\
&+ \frac{1}{2}\left(\frac{1}{10}\frac{dP^{9F}_{\rm iuud}}{dx_F} + \frac{2}{22}\frac{dP^{9C}_{\rm iuud}}{dx_F}\right) + \frac{1}{2}\left(\frac{1}{10}\frac{dP^{9F}_{\rm iudd}}{dx_F} + \frac{3}{22}\frac{dP^{9C}_{\rm iudd}}{dx_F}\right) \\
&+ \frac{1}{2}\left(\frac{1}{10}\frac{dP^{9F}_{\rm iddd}}{dx_F} + \frac{4}{22}\frac{dP^{9C}_{\rm iddd}}{dx_F}\right) + \frac{1}{2}\left(\frac{1}{10}\frac{dP^{9F}_{\rm isuu}}{dx_F} + \frac{3}{28}\frac{dP^{9C}_{\rm isuu}}{dx_F}\right) \\
&+ \frac{1}{2}\left(\frac{1}{10}\frac{dP^{9F}_{\rm isud}}{dx_F} + \frac{6}{28}\frac{dP^{9C}_{\rm isud}}{dx_F}\right) + \frac{1}{2}\left(\frac{1}{10}\frac{dP^{9F}_{\rm isdd}}{dx_F} + \frac{9}{28}\frac{dP^{9C}_{\rm isdd}}{dx_F}\right) \\
&+ \frac{1}{2}\left(\frac{1}{10}\frac{dP^{9F}_{\rm issu}}{dx_F} + \frac{6}{31}\frac{dP^{9C}_{\rm issu}}{dx_F}\right) + \frac{1}{2}\left(\frac{1}{10}\frac{dP^{9F}_{\rm issd}}{dx_F} + \frac{12}{31}\frac{dP^{9C}_{\rm issd}}{dx_F}\right) \\
&+ \frac{1}{2}\left(\frac{1}{10}\frac{dP^{9F}_{\rm isss}}{dx_F} + \frac{12}{37}\frac{dP^{9C}_{\rm isss}}{dx_F}\right), \qquad \text{(A.7)}
\end{aligned}$$

$$\begin{aligned}
\frac{dP^{\Xi^-}_{\Xi^-}}{dx_F} &= \frac{1}{6}\frac{dP^{5C}_{\rm iu}}{dx_F} + \frac{2}{6}\frac{dP^{5C}_{\rm id}}{dx_F} + \frac{3}{7}\frac{dP^{5C}_{\rm is}}{dx_F} + \frac{1}{13}\frac{dP^{7C}_{\rm iuu}}{dx_F} + \frac{2}{13}\frac{dP^{7C}_{\rm iud}}{dx_F} + \frac{3}{13}\frac{dP^{7C}_{\rm idd}}{dx_F} \\
&+ \frac{3}{16}\frac{dP^{7C}_{\rm isu}}{dx_F} + \frac{6}{16}\frac{dP^{7C}_{\rm isd}}{dx_F} + \frac{6}{17}\frac{dP^{7C}_{\rm iss}}{dx_F} + \frac{1}{22}\frac{dP^{9C}_{\rm iuuu}}{dx_F} + \frac{2}{22}\frac{dP^{9C}_{\rm iuud}}{dx_F} \\
&+ \frac{3}{22}\frac{dP^{9C}_{\rm iudd}}{dx_F} + \frac{4}{22}\frac{dP^{9C}_{\rm iddd}}{dx_F} + \frac{3}{28}\frac{dP^{9C}_{\rm isuu}}{dx_F} + \frac{6}{28}\frac{dP^{9C}_{\rm isud}}{dx_F} + \frac{9}{28}\frac{dP^{9C}_{\rm isdd}}{dx_F} \\
&+ \frac{6}{31}\frac{dP^{9C}_{\rm issu}}{dx_F} + \frac{12}{31}\frac{dP^{9C}_{\rm issd}}{dx_F} + \frac{12}{37}\frac{dP^{9C}_{\rm isss}}{dx_F}. \qquad \text{(A.8)}
\end{aligned}$$

Finally, we give the Ω distribution from a Ξ^- projectile,

$$\begin{aligned}
\frac{dP^{\Xi^-}_{\Omega}}{dx_F} &= \frac{1}{10}\frac{dP^{5F}_{\rm iu}}{dx_F} + \frac{1}{10}\frac{dP^{5F}_{\rm id}}{dx_F} + \frac{1}{2}\left(\frac{1}{10}\frac{dP^{5F}_{\rm is}}{dx_F} + \frac{1}{7}\frac{dP^{5C}_{\rm is}}{dx_F}\right) + \frac{1}{10}\frac{dP^{7F}_{\rm iuu}}{dx_F} \\
&+ \frac{1}{10}\frac{dP^{7F}_{\rm iud}}{dx_F} + \frac{1}{10}\frac{dP^{7F}_{\rm idd}}{dx_F} + \frac{1}{2}\left(\frac{1}{10}\frac{dP^{7F}_{\rm isu}}{dx_F} + \frac{1}{16}\frac{dP^{7C}_{\rm isu}}{dx_F}\right)
\end{aligned}$$

$$
\begin{aligned}
&+\frac{1}{2}\left(\frac{1}{10}\frac{dP^{7F}_{\mathrm{isd}}}{dx_F}+\frac{1}{16}\frac{dP^{7C}_{\mathrm{isd}}}{dx_F}\right)+\frac{1}{2}\left(\frac{1}{10}\frac{dP^{7F}_{\mathrm{iss}}}{dx_F}+\frac{3}{17}\frac{dP^{7C}_{\mathrm{iss}}}{dx_F}\right)\\
&+\frac{1}{10}\frac{dP^{9F}_{\mathrm{iuuu}}}{dx_F}+\frac{1}{10}\frac{dP^{9F}_{\mathrm{iuud}}}{dx_F}+\frac{1}{10}\frac{dP^{9F}_{\mathrm{iudd}}}{dx_F}+\frac{1}{10}\frac{dP^{9F}_{\mathrm{iddd}}}{dx_F}\\
&+\frac{1}{2}\left(\frac{1}{10}\frac{dP^{9F}_{\mathrm{isuu}}}{dx_F}+\frac{1}{28}\frac{dP^{9C}_{\mathrm{isuu}}}{dx_F}\right)+\frac{1}{2}\left(\frac{1}{10}\frac{dP^{9F}_{\mathrm{isud}}}{dx_F}+\frac{1}{28}\frac{dP^{9C}_{\mathrm{isud}}}{dx_F}\right)\\
&+\frac{1}{2}\left(\frac{1}{10}\frac{dP^{9F}_{\mathrm{isdd}}}{dx_F}+\frac{1}{28}\frac{dP^{9C}_{\mathrm{isdd}}}{dx_F}\right)+\frac{1}{2}\left(\frac{1}{10}\frac{dP^{9F}_{\mathrm{issu}}}{dx_F}+\frac{3}{31}\frac{dP^{9C}_{\mathrm{issu}}}{dx_F}\right)\\
&+\frac{1}{2}\left(\frac{1}{10}\frac{dP^{9F}_{\mathrm{issd}}}{dx_F}+\frac{3}{31}\frac{dP^{9C}_{\mathrm{issd}}}{dx_F}\right)+\frac{1}{2}\left(\frac{1}{10}\frac{dP^{9F}_{\mathrm{isss}}}{dx_F}+\frac{10}{37}\frac{dP^{9C}_{\mathrm{isss}}}{dx_F}\right), \qquad \text{(A.9)}
\end{aligned}
$$

$$
\begin{aligned}
\frac{dP^{\Xi^-}_{\Omega}}{dx_F} &= \frac{1}{7}\frac{dP^{5C}_{\mathrm{is}}}{dx_F}+\frac{1}{16}\frac{dP^{7C}_{\mathrm{isu}}}{dx_F}+\frac{1}{16}\frac{dP^{7C}_{\mathrm{isd}}}{dx_F}+\frac{3}{17}\frac{dP^{7C}_{\mathrm{iss}}}{dx_F}+\frac{1}{28}\frac{dP^{9C}_{\mathrm{isuu}}}{dx_F}\\
&+\frac{1}{28}\frac{dP^{9C}_{\mathrm{isud}}}{dx_F}+\frac{1}{28}\frac{dP^{9C}_{\mathrm{isdd}}}{dx_F}+\frac{3}{31}\frac{dP^{9C}_{\mathrm{issu}}}{dx_F}+\frac{3}{31}\frac{dP^{9C}_{\mathrm{issd}}}{dx_F}+\frac{10}{37}\frac{dP^{9C}_{\mathrm{isss}}}{dx_F}. \qquad \text{(A.10)}
\end{aligned}
$$

References

[1] E.M. Aitala, et al., E791 Collaboration, Phys. Lett. B 371 (1996) 157.
[2] M. Aguilar-Benitez, et al., LEBC-EHS Collaboration, Phys. Lett. B 161 (1985) 400.
[3] M. Aguilar-Benitez, et al., LEBC-EHS Collaboration, Z. Phys. C 31 (1986) 491.
[4] S. Barlag, et al., ACCMOR Collaboration, Z. Phys. C 49 (1991) 555.
[5] M.I. Adamovich, et al., WA82 Collaboration, Phys. Lett. B 305 (1993) 402.
[6] G.A. Alves, et al., E769 Collaboration, Phys. Rev. Lett. 72 (1994) 812.
[7] R. Werding, WA89 Collaboration, in: Proceedings of ICHEP94, 27th International Conference on High Energy Physics, Glasgow, Scotland, 1994.
[8] M.I. Adamovich, et al., WA89 Collaboration, Eur. Phys. J. C 8 (1999) 593.
[9] E. Ramberg, SELEX Collaboration, in: C.S. Kalman, et al. (Eds.), Hyperons, Charm and Beauty Hadrons, Proceedings of the 2nd International Conference on Hyperons, Charm and Beauty Hadrons, Montreal, Canada, 1996, Nucl. Phys. B (Proc. Suppl.) A 55 (1997) 173.
[10] J. Engelfried, et al., in: Proceedings of the 5th Workshop on Heavy Quarks at Fixed Target, Rio de Janeiro, Brazil, 2000, hep-ex/0012004.
[11] M. Bourquin, et al., Nucl. Phys. B 153 (1979) 13.
[12] M. Bourquin, et al., Z. Phys. C 5 (1980) 275.
[13] M. Bourquin, J.P. Repellin, Phys. Rep. 114 (1984) 99.
[14] S.F. Biagi, et al., Z. Phys. C 34 (1987) 187.
[15] O. Schneider, et al., Z. Phys. C 46 (1990) 341.
[16] A. Beretvas, et al., Phys. Rev. D 34 (1986) 53.
[17] M.I. Adamovich, et al., WA89 Collaboration, Z. Phys. C 76 (1997) 35.
[18] J.F. Gunion, Phys. Lett. B 88 (1979) 150.
[19] W.M. Geist, Nucl. Phys. A 525 (1991) 149c.
[20] T.R. Cardello, et al., Phys. Rev. D 32 (1985) 1.
[21] D.S. Barton, et al., Phys. Rev. D 27 (1983) 2580.
[22] P. Skubic, et al., Phys. Rev. D 18 (1978) 3115.
[23] S.J. Brodsky, P. Hoyer, C. Peterson, N. Sakai, Phys. Lett. B 93 (1980) 451.
[24] S.J. Brodsky, C. Peterson, N. Sakai, Phys. Rev. D 23 (1981) 2745.
[25] R. Vogt, S.J. Brodsky, Nucl. Phys. B 438 (1995) 261.

[26] R. Vogt, S.J. Brodsky, Nucl. Phys. B 478 (1996) 311.
[27] T. Gutierrez, R. Vogt, Nucl. Phys. B 539 (1999) 189.
[28] T.D. Gutierrez, R. Vogt, Nucl. Phys. A 705 (2002) 396.
[29] J. Smith, R. Vogt, Z. Phys. C 75 (1997) 271.
[30] N. Kidonakis, E. Laenen, S. Moch, R. Vogt, Phys. Rev. D 67 (2003) 074037.
[31] M. Glück, E. Reya, A. Vogt, Z. Phys. C 67 (1995) 433.
[32] M. Glück, E. Reya, I. Schienbein, Eur. Phys. J. C 10 (1999) 313.
[33] R. Vogt, S.J. Brodsky, P. Hoyer, Nucl. Phys. B 383 (1992) 643.
[34] R.K. Ellis, in: (Ed.) E.C. Brennan, Physics at the 100 GeV Scale, Proceedings of the 17th SLAC Summer Institute Stanford, California, 1989, SLAC Report No. 361 p. 45.
[35] B.L. Combridge, Nucl. Phys. B 151 (1979) 429.
[36] P. Nason, S. Dawson, R.K. Ellis, Nucl. Phys. B 303 (1988) 607.
[37] R. Vogt, Heavy Ion Phys. 17 (2003) 75.
[38] P. Hoyer, D.P. Roy, Phys. Lett. B 410 (1997) 63.
[39] C. Caso, et al., Eur. Phys. J. C 3 (1998) 1.
[40] R. Vogt, S.J. Brodsky, P. Hoyer, Nucl. Phys. B 360 (1991) 67.
[41] M.J. Leitch, et al., E789 Collaboration, Phys. Rev. Lett. 72 (1994) 2542.
[42] J. Badier, et al., NA3 Collaboration, Z. Phys. C 20 (1983) 101.
[43] M. Arneodo, Phys. Rep. 240 (1994) 301.
[44] K.J. Eskola, V.J. Kolhinen, P.V. Ruuskanen, Nucl. Phys. B 535 (1998) 351.
[45] K.J. Eskola, V.J. Kolhinen, C.A. Salgado, Eur. Phys. J. C 9 (1999) 61.
[46] http://cpt19.dur.ac.uk/cgi-hepdata/hepreac/1637169.